ISSN 1674-1056
http://cpb.iphy.ac.cn
http://iopscience.iop.org/cpb
中国物理 B
Chinese Physics
中国物理 Chinese Physics B

Molecular dynamics simulations of membrane deformation induced by amphiphilic helices of Epsin, Sar1p, and Arf1

Zhen-Lu Li(李振鲁)
Citation: Chin. Phys. B . 2018, 27(3): 038703. **doi:** 10.1088/1674-1056/27/3/038703

Journal homepage: http://cpb.iphy.ac.cn; http://iopscience.iop.org/cpb

What follows is a list of articles you may be interested in

Protein-membrane interactions investigated with surface-induced fluorescence attenuation

Li Ma(马丽), Ying Li(李颖), Ming Li(李明), Shuxin Hu(胡书新)
Chin. Phys. B . 2017, 26(12): 128708. **doi:** 10.1088/1674-1056/26/12/128708

Anisotropic formation mechanism and nanomechanics for the self-assembly process of cross-*β* peptides

Li Deng(邓礼), Yurong Zhao(赵玉荣), Peng Zhou(周鹏), Hai Xu(徐海), Yanting Wang(王延颋)
Chin. Phys. B . 2017, 26(12): 128701. **doi:** 10.1088/1674-1056/26/12/128701

A damping boundary condition for atomistic-continuum coupling

Jie Zhang(张杰), Kiet Tieu, Guillaume Michal, Hongtao Zhu(朱洪涛), Liang Zhang(张亮), Lihong Su(苏利红), Guanyu Deng(邓关宇), Hui Wang(王辉)
Chin. Phys. B . 2017, 26(6): 068702. **doi:** 10.1088/1674-1056/26/6/068702

Multiscale molecular dynamics simulations of membrane remodeling by Bin/Amphiphysin/Rvs family proteins

Chun Chan(陈骏), Haohua Wen(文豪华), Lanyuan Lu(鲁兰原), Jun Fan(范俊)
Chin. Phys. B . 2016, 25(1): 018707. **doi:** 10.1088/1674-1056/25/1/018707

Coupling of two-dimensional atomistic and continuum models for dynamic crack

Ren Guo-Wu, Tang Tie-Gang
Chin. Phys. B . 2014, 23(11): 118704. **doi:** 10.1088/1674-1056/23/11/118704

Molecular dynamics simulations of membrane deformation induced by amphiphilic helices of Epsin, Sar1p, and Arf1*

Zhen-Lu Li(李振鲁)[1,2,†]

[1] Department of Physiology and Biophysics, Case Western Reserve University, Cleveland 44106, USA
[2] Department of Physics, Nanjing University, Nanjing 210093, China

(Received 24 October 2017; revised manuscript received 12 December 2017; published online 13 February 2018)

The *N*-terminal amphiphilic helices of proteins Epsin, Sar1p, and Arf1 play a critical role in initiating membrane deformation. The interactions of these amphiphilic helices with the lipid membranes are investigated in this study by combining the all-atom and coarse-grained simulations. In the all-atom simulations, the amphiphilic helices of Epsin and Sar1p are found to have a shallower insertion depth into the membrane than the amphiphilic helix of Arf1, but remarkably, the amphiphilic helices of Epsin and Sar1p induce higher asymmetry in the lipid packing between the two monolayers of the membrane. The insertion depth of amphiphilic helix into the membrane is determined not only by the overall hydrophobicity but also by the specific distributions of polar and non-polar residues along the helix. To directly compare their ability to deform the membrane, the coarse-grained simulations are performed to investigate the membrane deformation under the insertion of multiple helices.

Keywords: cell membrane, amphiphilic helix, membrane deformation, molecular simulation

PACS: 87.15.kt, 87.14.ef, 87.14.ep, 87.15.ap **DOI:** 10.1088/1674-1056/27/3/038703

1. Introduction

The transports of cargo molecules in both endocytic and secretory pathways are conducted by coated vesicles. The formation of these vesicles involves many membrane remodeling proteins, such as the well-known coat proteins including clathrin in endocytic vesicle and contator in COPII and COPI transport vesicle.[1–3] However, clathrin, COPII, or COPI is not in direct contact with the membrane. Instead, there is a kind of protein which anchors to the membrane directly and can trigger an initial membrane deformation. Then, they further recruit membrane remodeling proteins (such as clathrin, COPII, or COPI) from the cytoplasm to generate membrane invagination or budding. Epsin is a representative one of such proteins, and is involved in the clathrin-mediated endocytic pathways.[4] Similarly, upon exchange of GDP to GTP, small GTPase Sar1p and Arf1 initiate the membrane bending during COPII and COPI transport pathway separately.[5,6]

The localization of Epsin, Sar1p, or Arf1 at the membrane is achieved by embedding its short *N*-terminal amphiphilic helix shallowly into one leaflet of the lipid membrane. In vitro experiments revealed that the association of Epsin, Sar1p, or Arf1 with the membrane could deform the membrane. For example, Epsin could convert PI(4,5)P_2 containing-liposomes into tubules with a diameter of 19 nm.[7] In the GTP-bound state, Sar1p could convert liposomes into tubules with a mean diameter of 26 nm,[8] and the myristoylated Arf1 could transform negatively-charged liposomes into tubules of 45 nm in diameter.[9] All these proteins show the ability to curve membrane into a bud or a tube with a size of a few tens of nanometers both in vitro and in vivo experiments. It is very important to clarify how these proteins deform the membrane, which could help better understand the generation of cellular traffic vesicles.

It is known that the *N*-terminal amphiphilic helices of proteins like Espin, Sar1p, and Arf1 play a crucial role in inducing membrane deformation.[10–12] The *N*-terminal amphiphilic helix is embedded into the lipid matrix, with their hydrophobic face inserting between fatty acyl-chain and their polar face exposing to the water. The so-called local spontaneous curvature mechanism (or hydrophobic inserting mechanism) reveals that a shallow insertion of an amphiphilic helix into only one leaflet of the membrane can perturb the packing of the lipid polar headgroups and induce a local monolayer deformation.[10,11] Theoretical work by Campelo *et al.* indicated that the insertion of amphiphilic helices can be very powerful in bending the membrane, and shallow insertions are best suited for the production of high membrane curvature.[13]

Membrane-interacting peptides are also used in the development of novel antimicrobial agents.[14,15] Or in some cases, the membrane penetration property of peptides is used to design the drug transport vectors across cell membrane.[16–18] However, peptide may also disrupt the integrity of cell membrane. The merits and side effects need to be kept in balance in the design of drug transport vectors.[19] Characterization of the detailed peptide–membrane interactions is vital for understanding the molecular mechanism and biological

*Project supported by the National Natural Science Foundation of China (Grant Nos. 91427302 and 11474155).
†Corresponding author. E-mail: zxl480@case.edu
© 2018 Chinese Physical Society and IOP Publishing Ltd

function, and for designing functional peptide materials.[20,21] Computational study has been a tool of particular importance in revealing the molecular mechanism of peptide–membrane interaction.[22–25] For membrane remodeling amphiphilic helices, so far, many simulation researches have focused on the N-BAR domain, as the dimer of this protein has both a charged, crescent-shaped surface and two amphiphilic helices, which may bend the membrane through combining a scaffold mechanism and the hydrophobic inserting mechanism.[26–31] Recently, the membrane remodeling effects of anti-bacteria peptides[15] and monomeric α-Synuclein[32] that are involved in the mitochondrial remodeling were also studied. However, to the best of our knowledge, the role of these amphiphilic helices of Epsin (1-MSTSSLRRQMKNIVHN-16), Sar1p(1MAGWDIFGWFRDVLASLGLWNKH-23) and Arf1 (2-GNIFANLFKGLFGKK-16) in generating membrane deformation have not been investigated in previous computational studies. Actually, though participating in rather different cellular transport processes, Epsin, Sar1p, and Arf1 share a similar mechanism that upon stimulus of signaling lipids or nucleotide, the *N*-terminal segments of Epsin, Sar1p, or Arf1 fold into an amphiphilic helix and insert into the membrane. Therefore, it is also of great importance to reveal the similarity and difference between their interactions with cell membrane.

In the present work, the molecular mechanisms of the amphiphilic helices of Epsin, Sar1p, and Arf1 deforming the membrane are studied by combining the all-atom and coarse-grain simulations. The all-atom simulations are performed to investigate the complex of a single helix associated with the membrane. Particularly, the influence of the helix insertion on the lipid packing of the membrane is analyzed. The coarse-grained simulations on a large scale are performed in order to directly illustrate the membrane deformation process under the insertion of multiple helices into the membrane.

2. Model and methods

In the all-atom (AA) simulations, a membrane of 84 DOPC (1,2-Dioleoyl-sn-glycero-3-phosphocholine) and 36 DOPS (1,2-di-(9Z-octadecenoyl)-sn-glycero-3-phospho-L-serine) molecules was prepared. Certain quantities of anionic lipids (30%) were added into the membrane, as done in several previous studies.[28–30,32] The membrane was equilibrated for 100 ns before further application. The *N*-terminal helices of Epsin, Sar1p, and Arf1 were all equilibrated for 10 ns in solvents, and the final configurations are shown in Fig. 1(a). The corresponding helical wheel representations for these helices are shown in Fig. 1(b). Next, the helix was pre-inserted into the membrane by using the InflatGro method,[33,34] with its hydrophobic face interacting with the membrane interior while the hydrophilic face interacting with the water. In order to enhance simulation sampling, for each kind of helix of Epsin, Sar1p, and Arf1, two different initial simulation configurations of the helix relative to the membrane were adopted, by displacing the helix with its long axis either parallel to the *x*-axis or parallel to the *y*-axis of the simulation box. Water molecules were then added to the system. The charges of DOPS molecules and the amphiphilic helix were neutralized by adding appropriate number of counter-ions. A restrained NVT equilibrium simulation (the mainchain Cα atoms are restrained) of 1 ns and a followed restrained NPT simulation of 40 ns were performed to relax the simulation system. The unstrained run was performed for 360 ns for analysis.

The CHARMM36 all-atom force field was used for the phospholipids as well as the amphiphilic helix (the histidine is in neutral form).[35,36] The TIP3P model was used for water.[37] The electrostatic interactions were treated by particle-mesh Ewald (PME) method with a real-space cutoff of 1.2 nm.[38] The van der Waals interactions were also cut at 1.2 nm. Bond lengths were constrained via the P-LINCS algorithm.[39] A time step of 2 fs was employed. The center of mass motion was removed in each step, and the neighbor list was updated in every 10 steps. The temperature was coupled by using Nose–Hoover thermostat at 310 K, whereas the pressure control was achieved by semi-isotropic Parrinello–Rahman scheme at 1 bar.[40]

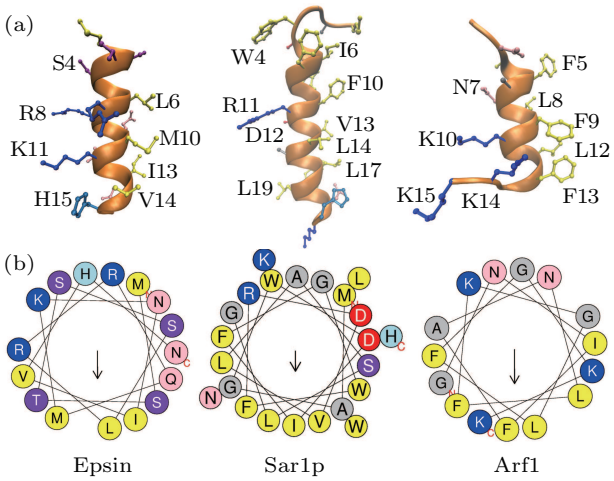


Fig. 1. (color online) (a) Configurations and (b) corresponding helical wheel representations of the amphiphilic helices of Epsin, Sar1p, and Arf1. Color coding for residues: yellow for hydrophobic, purple for serine and threonine, blue for basic, red for acidic, pink for asparagine and glutamine, grey for alanine and glycine, green for proline, and light blue for histidine. The arrow in helical wheels corresponds to the hydrophobic moment.

The MARTINI coarse-grained force field (including the improved protein force filed) developed by Marrink's group, was used for the coarse-grained (CG) simulations.[41–43] In the improved MARTINI protein force field, the polarized water was used and the residues were reparametrized through reassignment of bead types or by introducing embedded charges. These procedures made the force field better to describe the

peptide–membrane interactions. The Lennard–Jones (LJ) potentials were cut at a distance of 1.2 nm and smoothly shifted to zero between 0.9 and 1.2 nm. The electrostatic interactions were also cut at a distance of 1.2 nm with the smooth switching of the interactions from 0.0 to 1.2 nm. The relative dielectric constant was set to be 1. A large rectangular membrane consisting of 3024 DOPC and 1296 DOPS was prepared, and the simulation box was about 110 nm in the X-axis direction and about 14 nm in the Y-axis direction. Twenty helical peptides were pre-inserted into the membrane with their long axis along the Y direction.[28] The interval space between helices is about 2 nm along the X direction. About 190000 polarized water molecules were added to the system, and counter-ions were included to neutralize the charge of DOPS and helices separately. The coarse-grained simulations were performed in the NPT ensembles coupling to a bath with a constant temperature T of 310 K and a constant pressure P of 1 bar.[40] A time step of 20 fs was used in the CG simulations. Notice that the effective time sampled in CG simulations is 4 times as large as that in atomistic simulations, so here the effective simulation time step is approximately 80 fs.[44] For each CG simulation, a simulation of 2 μs was performed.

All the all-atom and coarse-grained simulations and the analysis were performed by using GROMACS 4.6.5 software package.[40]

3. Results and discussion

3.1. Partitioning of amphiphilic helices in the membrane

Figure 2 shows the final configurations of the N-terminal helices of Epsin, Sar1p, and Arf1 binding to the membrane as well as the density distributions of the lipid (P or C2 atoms) and the helical peptide (backbone atoms). The helices are roughly parallel to the membrane surface and embedded into the lipid matrix partially. The center of mass of the backbone atoms of these helices is at the level of the lipid glycerol group. Specifically, for Epsin and Sar1p, the amphiphilic helix is distributed between the lipid glycerol group (C2) and phosphate group (P), while for Arf1, it is below the average position of glycerol group (C2). Figure 3(a) further shows the time evolutions of the distances of these amphiphilic helices to the membrane center. Starting from a similar initial displacement, these helices gradually adjust themselves to their most preferred distribution. As shown in Table 1, the averaged insertion depth of the helix of Arf1 is the deepest (about 1.52 nm from the membrane center), while the N-terminal helices of the Epsin and Sar1p have shallower insertion depths of about 1.96 and 1.83 nm, respectively.

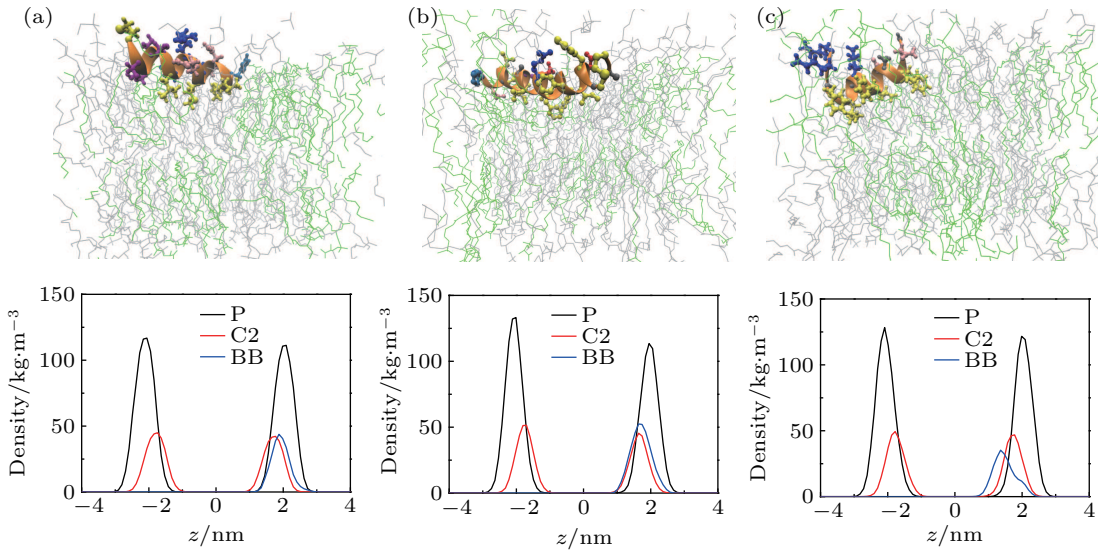


Fig. 2. (color online) (a) Top: final configuration of N-terminal helix of Epsin, Sar1p, and Arf1 binding to the membrane. DOPC is in grey and DOPS is in green. Color code for the helix is the same as those in Fig. 1. (b). Bottom: density distributions of lipid P and C2 atoms, and of the backbone (BB) atoms of the helix.

According to the experimental results, Epsin and Sar1p initiate membrane tubes with smaller diameter (compared to Arf1). So possibly a deep insertion depth of the amphiphilic helix into the membrane is not suited for bending the membranes. Instead, a shallow insertion depth into the membrane can be more efficient in creating high membrane curvature. This point is also indicated in several theoretical researches on the short peptide interacting with the membrane.[13,45] In particular, theoretical work by Campelo *et al.* showed that for a membrane with monolayer thickness values of 2.0 nm and 2.2 nm, the optimal insertion depths of the helix (where the helix can initiate the largest membrane spontaneous curvature) are about 1.75 nm and 1.9 nm from the membrane center respectively.[13] Here, in our simulations, the thickness of the membrane (measured from the peaks of the phosphate distribution) is about 4.10 nm. The half-thickness of the membrane (the monolayer thickness) is 2.05 nm. Supposing that the largest membrane spontaneous curvature caused by embedded

inclusions is linearly dependent on the monolayer thickness, the optimal insertion depth of inclusion for a membrane with monolayer thickness of 2.05 nm is estimated at 1.8 nm, based on the results of Campelo *et al.*[13] The insertion depth of the helix of Arf1 is 1.52 ± 0.09 nm, much lower than 1.8 nm. The insertion depths of the *N*-terminal helices of Epsin and Sar1p are 1.96 ± 0.08 nm and 1.83 ± 0.08 nm respectively, which are closer to 1.8 nm. The peptide is simplified as a simple cylinder in the theoretical model,[13] while in the molecular simulation, it considers the full atomic details. Besides, in the simulation, the positions of these helices also undergo essential fluctuation. These factors may lead to discrepancies between the theoretical prediction and molecular simulation. Nevertheless, the results of the theoretical prediction and molecular simulations are comparable. This means that a deep insertion of the helix into the membrane slightly contributes to the membrane deformation, while a shallow insertion of the helix at the level of (or slightly above) membrane hydrophilic-hydrophobic interface is suitable for bending the membrane. Taken together the theoretical results of Campelo *et al.*[13] and simulation results here, an insertion depth from 1.75 nm to 2.0 nm should be suitable for producing high membrane curvature.

3.2. Factors influencing insertion depth of amphiphilic helices into membrane

Figures 3(b) and 3(c) show the pair interactions between the amphiphilic helix and the membrane. The Van der Waals interaction between the helix of Sar1p and the membrane is the lowest. The values are almost twice and 1.5 times lower than the interactions between the membrane and the helix of Epsin, and between the membrane and the helix of Arf1 respectively. This is partly due to the longer sequence length of the helix of Sar1p (1.4 times larger than the helix of Epsin and 1.5 times larger than the helix of Arf1; see Table 1). More importantly, the high hydrophobicity of Sar1p considerably contributes to the low Van der Waals interaction. In contrast, the electrostatic interactions of the helices of the Epsin and Arf1 with the membrane are much lower than the helix of Sar1p. The averaged electrostatic interactions energy (averaged over the course of the last 200 ns trajectories) are -921 ± 117, -739 ± 112 and -585 ± 97 kcal/mol, respectively, between the membrane and the helices of Epsin, Arf1 and Sar1p. The helices of both Epsin and Arf1 have three net positive charges, while the helix of Sar1p has no net charge. Therefore, the former two helices have stronger electrostatic interactions with the anionic DOPS lipid molecules.

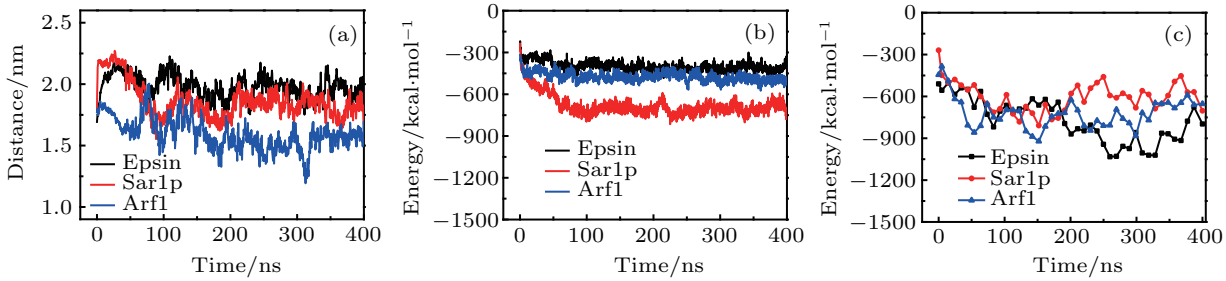


Fig. 3. (color online) (a) Time evolutions of the distance between the center of mass of the backbone atoms of the helices of Epsin, Sar1p and Arf1 and the center of mass of lipid membrane along the *Z* axis. ((b), (c)) Time evolutions of the Van der Waals and the electrostatic interaction between the lipid membrane and the helices of Epsin, Sar1p, and Arf1.

Table 1. Properties of the amphiphilic helices of Epsin, Sar1p, and Arf1. L is for sequence length, z for the net charge, H for the hydrophobicity, and μH for the hydrophobic moment. $D_{\rm h}$ denotes the insertion depth of the helix in the all atom simulations. $S^{\rm u}_{\rm CD}$ and $S^{\rm l}_{\rm CD}$ refer to the order parameters of the upper and lower leaflets in the all atom simulations (averaged over the last 200 ns). R denotes the estimated curvature radius of the membrane deformation induced by the insertion of multiple helices in the CG simulations. This value is taken averaged over the last 1 μs simulation.

Helix	L	z/e	H	μH	$D_{\rm h}$/nm	$S^{\rm u}_{\rm CD}$	$S^{\rm l}_{\rm CD}$	R/nm
Epsin	16	+3	0.131	0.483	1.96±0.08	0.136	0.162	59±6
Sar1p	23	0	0.707	0.270	1.83±0.08	0.125	0.162	55±8
Arf1	15	+3	0.447	0.424	1.52±0.09	0.149	0.160	152±68

A high hydrophobicity of peptide is favorable for the strong binding to the membrane and a deep insertion depth into the membrane. However, the insertion depth also depends on the interaction of polar and charge residues with the lipid headgroup and water.[46] Figure 4 shows the insertion depth of individual residues into the membrane. For each amphiphilic helix, the residues that have a relatively deep insertion into the membrane are mostly hydrophobic residues. These residues include L6, M10, I13, and V14 in the helix of Epsin, residues I6, F7, W9, F10, V13, L14, L17 in the helix of Sar1p and residues F5, L8, F9, L12, F13 in the helix of Arf1. Typically, residues at the bottom of the helix wheel in Fig. 1 (the hydrophobic face) have deep insertion into the lipid acyl chains, except that K15 and K16 (i.e., at the end of the helix of Arf1), are at lipid–water interface due to their favorable interactions with the lipid headgroup. In contrast with the hydrophobic

residues, polar and charge residues prefer to stay at the lipid–water interface, which are driven by the polar as well as electrostatic interaction with the lipid headgroup or water. Hydrogen bonds formed between the residues and the lipids are shown in Fig. 4. Remarkably, positively charged residues including arginine and lysine are largely involved in the hydrogen bond interaction with the lipid molecules (typically 1–2.5 hydrogen bonds for each). Polar residues also form hydrogen bonds with the lipid molecules, but to a less extent.

The distributions of polar and non-polar residues along the helix are of great importance in the insertion of the amphiphilic helix into the membrane. Supposing that an overall hydrophobic face has few polar residues incorporated (such as N20 in Sar1p), a deep insertion of the amphiphilic helix into the membrane will become unfavorable since the polar residues are unlikely to interact with the hydrophobic acyl chains of lipid. Regarding the amphiphilic helix of Sar1p, the hydrophobic and hydrophilic face of the helix are mixed with few polar and non-polar residues respectively. Even though the helix of Sar1p has a high hydrophobicity, the helix only has a modest insertion depth into the membrane. To quantitatively depict the amphiphilicity of a helical peptide, the hydrophobic moment (μH) was calculated,[47] showing whether a helix exhibits clearly one hydrophobic face and one polar face. A large μH value means that the helix is amphiphilic perpendicular to its axis. Though being highly hydrophobic, the helix of Sar1p only has a low μH due to the doping of polar residues at its hydrophobic face and nonpolar residues at its hydrophilic face. The helix of Arf1 has medium hydrophobicity and μH (see Table 1). Excluding the two lysines (K15K16) at the end of the helix of Arf1, the hydrophobic face of the helix of Arf1 is wide and clear. These features contribute to the deepest insertion depth into the membrane for the helix of Arf1. The helix of Epsin has large μH but very low hydrophobicity. The hydrophobic face of the helix of Epsin is very small, therefore it only has a shallow insertion depth into the membrane.

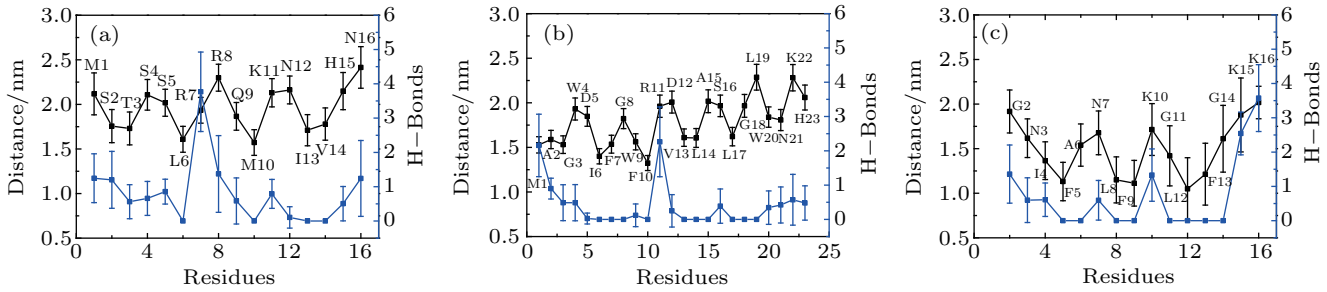


Fig. 4. (color online) Average insertion depths of individual residues into the membranes (black line) and the numbers of hydrogen bonds formed between residues and the lipid membranes (blue line). Hydrogen bonds are counted between a donor atom (D) and an acceptor atom (A) provided that the distance (D–A) is less than 3.5 Å and the angle (D–H–A) is less than 30° Panels (a)–(c) are for the *N*-terminal helices of Epsin, Sar1p, and Arf1, respectively.

3.3. Effect of amphiphilic helices on lipid packing of the membrane

The insertion of the helix will influence the lipid packing of membrane. This effect can be studied by calculating the deuterium order parameter (S_{CD}) of the lipid acyl chain. For each amphiphilic helix, the order parameter is shown in Figs. 5(a) and 5(b) for the upper leaflet (containing the helix) and the lower leaflet respectively. The order parameter for the upper leaflet in the presence of *N*-terminal helices of Epsin and Sar1p decreases a lot compared with for a pure membrane, while for the helix of Arf1, the value nearly has no change in spite of its deep insertion into the membrane. Oppositely, as for the lower leaflet without an embedded helix, the order parameter has an approximately equal increase for each system. This indicates that the insertion of the helix into one leaflet has nonnegligible influence on the opposite leaflet of the membrane. This is reasonable by considering the coupling between the two leaflets of membrane — the opposite leaflet makes corresponding adjustment to the changes in the packing of acyl chains of the upper leaflet. Thus, the asymmetry in the order parameter of the two leaflets could be an important driving force for the membrane deformation.[32,48] The asymmetry in the lipid packing of the two leaflets probably implies an asymmetry in the stress pressure for the two leaflets, and an asymmetric stress pressure profile results in the generation of membrane deformation.

As shown in Table 1, the order parameter asymmetry induced by the insertion of the helices of Epsin and Sar1p into the membrane is much larger than the insertion of the helix of Arf1. This is likely to be related to the high efficiencies of Epsin and Sar1p in creating membrane deformation. On the basis of above results, the insertion of amphiphilic helix into the membrane induces an asymmetry in the lipid packing of the two leaflets of membrane, which further initiates the membrane deformation. Moreover, a relatively shallow insertion depth into the membrane is more efficient in generating high asymmetry in the lipid packing. The extent of the asymmetry in the lipid packing induced by the amphiphilic helix is positively correlated with the efficiency of the helix in producing membrane curvature.

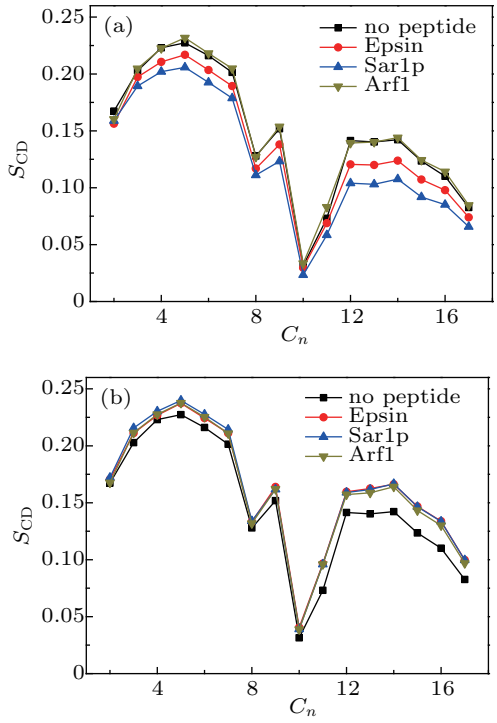


Fig. 5. (color online) Deuterium order parameters of the lipid acyl chain for (a) upper leaflet and (b) lower leaflet in the presence of different helices.

3.4. Membrane deformation induced by insertion of multiple helices

In experiment, typically multiple proteins cooperate together to create a membrane bud or tube. To investigate the membrane deformations in simulations with full atomic resolution is still challenging, considering the huge computing cost. In the meantime, coarse grained simulations using simplified representations of atoms can extend the simulations to a larger space scale and a longer time scale.[49–52] Simulation at multiple scales helps investigate the physical process at different levels, and it keeps the balance between the computing accuracy and cost.[53,54] In order to directly investigate the membrane bending when there are multiple helices inserted into the membrane, we conduct the coarse-grained simulation. A larger membrane with 4320 lipids is built in the coarse grain simulation with 20 amphiphilic helices inserted into the membranes.

After initially placing multiple helices into the membranes, the membranes are found to be deformed by these helices. Figure 6 shows the final configurations of multiple amphiphilic helices of Epsin, Sar1p, and Arf1 interacting with the membrane. In Fig. 6, the membranes bend into the area enclosed by the amphiphilic helices, and these amphiphilic helices spread on the area with distinguishable membrane deformations. The extent of membrane deformation is further measured by using the maximum curvature along the membrane that is covered by the amphiphilic helices.[28] Specifically, the coordinates of the CG beads of the lipid molecules are projected onto the x–z plane, and these projected scattered points are interpolated to estimate the membrane shape. The maximum curvature along the estimated membrane shape is used to characterize the degree of membrane deformation. The time evolutions of the maximum curvature under the insertion of the N-terminal helices of Epsin, Sar1p, and Arf1 are plotted

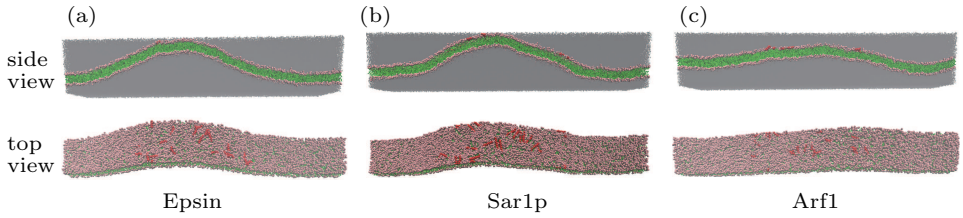


Fig. 6. (color online) Final configurations of multiple amphiphilic helices of Epsin, Sar1p and Arf1 interacting with the membrane.

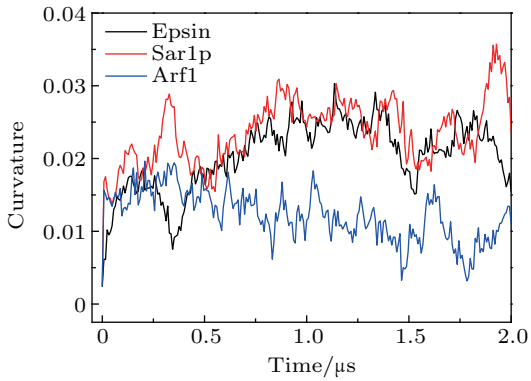


Fig. 7. (color online) Time evolutions of the mean curvature of the membrane segment enriched of amphiphlic helices of Epsin, Sar1p, or Arf1.

in Fig. 7. The mean value of the estimated curvature radii induced by the membrane insertion of the amphiphilic helices of Epsin, Sar1p, and Arf1 are 59 nm, 55 nm, 152 nm, respectively (see Table 1). This is consistent with the inference in the all-atom simulation, namely, the N-terminal helices of Epsin or Sar1p induce a much larger membrane curvature than those of the Arf1. Since the experimental conditions contain many other factors that are not easy to be considered in the molecular dynamics simulation,[7–9] these values are still not able to quantitatively compare with the sizes of buds or tubes induced by Epsin, Sar1p, and Arf1 in the experiments. Nevertheless, the general trends of the experiments and the results of all-atom, coarse-grained simulations here are similar to each other, i.e., Epsin and Sar1p are more powerful in generating membrane deformations.

4. Conclusions and perspectives

In this work, all-atom and coarse-grained molecular dynamics simulations are performed to study the interactions of *N*-terminal amphiphilic helices of Epsin, Sar1p, and Arf1 with the lipid membranes. In all-atom simulations, these amphiphilic helices are inserted by themselves shallowly into the lipid matrix, and induce an asymmetry in the lipid packing of the membrane. Importantly, a shallow rather than a deep insertion of the amphiphilic helix into the membrane is more suitable for generating high asymmetry in the lipid packing. Besides, the induced asymmetry in the lipid packing may be the driven force to deform membranes. Since the helices of Epsin and Sar1p each induce a larger asymmetry in the lipid packing than the helix of Arf1, the former two helices could produce a larger membrane deformation than the later one, which is verified in the coarse-grained simulations. Generally, the findings here are consist with the experimental results qualitatively so that Epsin and Sar1p are more powerful in bending the membrane. In terms of peptide design, a helical peptide with a narrow but clear hydrophobic face seems to be optimized for inducing the membrane deformation. Our findings here can enhance the understanding of the protein-driven membrane remodeling process.

Acknowledgment

We are grateful to the High Performance Computing Center (HPCC) of Nanjing University for performing the numerical calculations in this paper on its IBM Blade cluster system.

References

[1] Kirchhausen T 2000 *Nat. Rev. Mol. Cell Biol.* **1** 187
[2] Bonifacino J S and Schwartz J L 2003 *Nat. Rev. Mol. Cell Biol.* **4** 409
[3] Faini M, Beck R, Wieland F T and Briggs J A G 2013 *Trends Cell Biol.* **23** 279
[4] Chen H, Fre S, Slepnev V I, Capua M R, Takei K, Butler M H, Fiore P P D and Camilli P D 1988 *Nature* **394** 793
[5] Fath S, Mancias J D, Bi X and Goldberg J 2007 *Cell* **129** 1325
[6] Schorey C D S and Chavrier P 2006 *Nat. Rev. Mol. Cell Biol.* **7** 347
[7] Ford M G J, Mills I G, Peter B. J, Vallis Y, Praefcke G J K, Evans P R and McMahon H T 2002 *Nature* **419** 361
[8] Lee M C, Orci L, Hamamoto S, Futai E, Ravazzola M and Schekman R 2005 *Cell* **122** 605
[9] Krauss M, Jia J Y, Roux A, Beck R, Wieland F T, Camilli P D and Haucke V 2008 *J. Biol. Chem.* **283** 27717
[10] Zimmerberg J and Kozlov M M 2006 *Nat. Rev. Mol. Cell Biol.* **7** 9
[11] McMahon H T and Gallop J L 2005 *Nature* **438** 590
[12] Drin G and Antonny B 2010 *FEBS Lett.* **584** 1840
[13] Campelo F, McMahon H T and Kozlov M 2008 *Biophys. J.* **95** 2325
[14] Li Z L, Ding H M and Ma, Y Q 2016 *J. Phys.: Condens. Mat.* **28** 083001
[15] Woo H J and Wallqvist A 2011 *J. Phys. Chem. B* **115** 8122
[16] Li Z L, Ding H M and Ma Y Q 2013 *Soft Matter* **9** 1281
[17] Yue T T, Zhang X R and Huang F 2014 *Soft Matter* **10** 2024.
[18] He X C, Lin M, Sha B Y, Feng S S, Shi X H, Qu Z G and Xu F 2015 *Sci. Rep.* **5** 12808
[19] Ding H M and Ma Y Q 2017 *Nanoscale Horizons*
[20] Ma L, Li Y, Li M and Hu S 2017 *Chin. Phys. B* **26** 128708
[21] Zhang L, Hao C, Feng Y, Gao F, Lu X, Li J and Sun R 2016 *Chin. Phys. B* **25** 9
[22] Bond P J and Sansom M S P 2006 *J. Am. Chem. Soc.* **128** 2697
[23] Hu Y, Sinha S K and Patel S 2014 *J. Phys. Chem. B* **118** 11973
[24] Hu Y, Ou S and Patel S 2013 *J. Phys. Chem. B* **117** 11641
[25] He X C, Qu Z G, Xu F, Lin M, Wang J L, Shi X H and Lu T J 2014 *Soft Matter* **10** 139
[26] Peter B J, Kent H M, Mills I G, Vallis Y, Butler P J G, Evans P R and McMahon H T 2015 *Science* **303** 495
[27] Campelo F, Fabrikant G, McMahon H T and Kozlov M. 2010 *FEBS Lett.* **584** 1830
[28] Blood P D and Voth G A 2006 *Proc. Natl. Acad. Sci. U. S. A.* **103** 15068
[29] Cui H, Mim C, Vazquez F X, Lyman E, Unger V M and Voth G A 2013 *Biophys. J.* **104** 404
[30] Yin Y, Arkhipov A and Schulten K 2009 *Structure* **17** 882
[31] Chan C, Wen H, Lu L and Fan J 2015 *Chin. Phys. B* **25** 1
[32] Braun A R, Lacy M M, Ducas V C, Rhoades E and Sachs J N 2014 *J. Am. Chem. Soc.* **136** 9962
[33] Kandt C, Ash W L and Tieleman D P 2007 *Methods* **41** 475
[34] Schmidt T H and Kandt C 2012 *J. Chem. Inf. Model.* **52** 2657
[35] Klauda J B, Venable R M, Freites J A, O Connor J W, Mondragon-Ramirez C, Vorobyov I, Tobias D J, MacKerell A D and Pastor R W 2010 *J. Phys. Chem. B* **114** 7830
[36] Huang J and MacKerell A D 2010 *J. Comput. Chem.* **34** 2135
[37] Jorgensen W L and Madura J D 1983 *J. Am. Chem. Soc.* **105** 1407
[38] Essmann U, Perera L, Berkowitz M L, Darden T, Lee H and Pedersen L G 1995 *J. Chem. Phys.* **103** 8577
[39] Hess B 2008 *J. Chem. Theory Comput.* **4** 116
[40] Spoel D V D, Lindahl E, Hess B, Groenhof G, Mark A E and Berendsen H J C 2005 *J. Comput. Chem.* **26** 1701
[41] Yesylevskyy S O, Schafer L V, Sengupta D and Marrink S J 2010 *PLoS Comput. Biol.* **6** e1000810
[42] Marrink S J, Risselada H J, Yefimov S, Tieleman, D P and de Vires A H 2007 *J. Phys. Chem. B* **111** 7812
[43] de Jong D H, Singh G, Bennett W F D, Arnarez C, Wassenaar T A, Schafer L V, Periole X, Tieleman D P and Marrink S J 2013 *J. Chem. Theory Comput.* **9** 687
[44] Marrink S J, de Vries A H and Mark A E 2004 *J. Phys. Chem. B* **108** 750
[45] Zemel A, Ben-Shaul A, and May S 2008 *J. Phys. Chem. B* **112** 6988
[46] MacCallum J L, Bennett W F D and Tieleman D P 2008 *Biophys. J.* **94** 3393
[47] Eisenberg D, Weiss R M and Terwilliger T C 1982 *Nature* **299** 371
[48] Frolov V A and Zimmerberg, J 2010 *FEBS Lett.* **584** 1824
[49] Ding H M and Ma Y Q 2012 *Biomaterials* **33** 5798
[50] Nielsen S O, Bulo R E, Moore P B and Ensing B 2010 *Phys. Chem. Chem. Phys.* **12** 12401
[51] Yang K and Ma Y Q 2010 *Nat. Nanotechnol.* **5** 579
[52] Ding H M and Ma Y Q 2015 *ACS Nano* **6** 1230
[53] Ding H M and Ma Y Q 2015 *Small* **11** 1055
[54] Marrink S J and Tieleman D P 2013 *Chem. Soc. Rev.* **42** 6801